Available online at www.sciencedirect.com
ScienceDirect
Journal of Power Sources 176 (2008) 259–269
JOURNAL OF POWER SOURCES
www.elsevier.com/locate/jpowsour

Adaptive maximum power point tracking control of fuel cell power plants

Zhong Zhi-dan [a,b,*], Huo Hai-bo [a], Zhu Xin-jian [a], Cao Guang-yi [a], Ren Yuan [a]

[a] *Fuel Cell Research Institute, Shanghai Jiao Tong University, Shanghai 200030,China*
[b] *College of Electromechanical Engineering, Henan University of Science and Technology, Luoyan 471003, Henan Province, China*

Received 3 September 2007; received in revised form 23 October 2007; accepted 23 October 2007
Available online 4 November 2007

Abstract

A fuel cell's output power depends nonlinearly on the applied current or voltage, and there exists a unique maximum power point (MPP). This paper reports a first attempt to trace MPPs by an extremum seeking controller. The locus of MPPs varies nonlinearly with the unpredictable variations in the fuel cell's operation conditions. Thus, a maximum power point tracking (MPPT) controller is needed to continuously deliver the highest possible power to the load when variations in operation conditions occur. A two-loop cascade controller with an intermediate converter is designed to operate fuel cell power plants at their MPPs. The outer loop uses an adaptive extremum seeking algorithm to estimate the real-time MPP, and then gives the estimated value to the inner loop as the set-point, at which the inner loop forces the fuel cell to operate. The proposed MPPT control system provides a simple and robust control law that can keep the fuel cell working at MPPs in real time. Simulation shows that this control approach can yield satisfactory results in terms of robustness toward variations in fuel cell operation conditions.

Keywords: Fuel cell (FC); Power control; Maximum power point tracking (MPPT); Adaptive extremum seeking

1. Introduction

As a clean energy conversion technology, fuel cells are a promising alternative to a wide variety of power generation appliances. Due to its low operating temperature, high power density and fast startup, the proton exchange membrane (PEM) fuel cell power plant is a promising candidate for residential and vehicular applications. But fuel cells call for large amounts of investment. To minimize the overall system cost, the ability to extract the maximal power from a fuel cell is a crucial issue that must be considered for the optimal design of a fuel cell powered system [1].

When a fuel cell is directly connected to an external load, its output power depends on both the internal electro-chemical reaction and the external load impedance. The system's operating point is at the intersection of the fuel cell's I–P curve and the load line. There exists a unique operating point, called the maximum power point (MPP), at which the fuel cell produces its maximum power, as illustrated in Fig. 1. According to the power transfer theory, the power delivered to the load is maximized when the fuel cell internal impedance equals the load impedance. As either of the two impedances may vary, the chances are quite slim that the MPP happens to be the operating point. In most cases, it is actually undesirable to operate at the maximum power, because the corresponding fuel efficiency is at best 50%. But there are applications where power density is at a premium as compared with fuel efficiency, and the maximum power point tracking (MPPT) would be beneficial in such situations.

Extensive discussions on the fuel cell I–V characteristic, which can be found in the literature [2–4], show that the curve depends strongly on operating parameters in a nonlinear way. Mishra et al. did some valuable work on the manipulation of the fuel cell to attain the MPP. Firstly, they picked out a physics-

* Corresponding author at: Fuel Cell Research Institute, Shanghai Jiao Tong University, Shanghai 200030, China. Tel.: +86 21 62932154; fax: +86 21 62932154.
E-mail address: Johnsonzzd@gmail.com (Z.-d. Zhong).

0378-7753/$ – see front matter © 2007 Elsevier B.V. All rights reserved.
doi:10.1016/j.jpowsour.2007.10.080

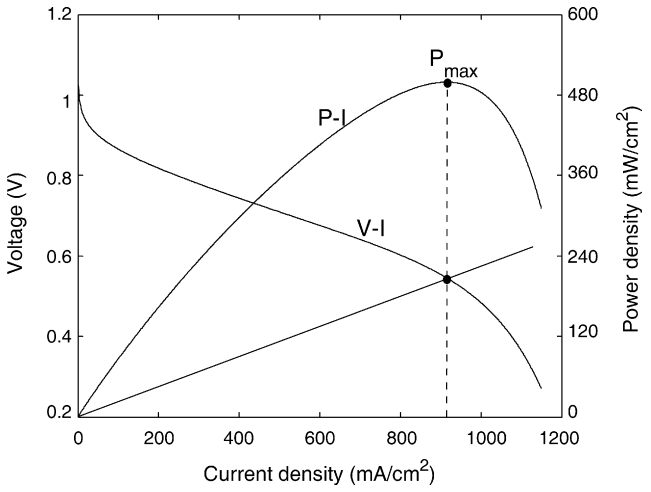

Fig. 1. Typical fuel cell polarization and power curves.

based model for fuel cell design and optimization [1]. Then, they made use of the model-based optimization methodology to determine the MPP of the proton exchange membrane (PEM) fuel cell, which is influenced by such operating parameters as the fuel cell temperature, the anode pressure, the cathode pressure, the relative anode humidity, the relative cathode humidity, the anode stoichiometry, the cathode stoichiometry, the anode dry gas mole fraction, and the cathode dry gas mole fraction [5]. In essence, they took an open loop approach. Hence the model mismatch caused by parametric uncertainties and disturbances is unavoidable. Also it is very hard to online determine whether the fuel cell is working at its MPP by measuring so many parameters. Most importantly, they neglected the other side of the coin: the external load.

Benziger et al. [6] noted that previous researchers had overlooked a decisive factor in the determination of the MPP, i.e., the external load. By adding a variable load to the base external load to achieve increased power output, they found that changing the external load impedance was a more effective method to alter the power delivery. It is well-known that maximum power occurs when the sum of the external impedance, i.e., the variable load impedance plus the base load impedance, is equal to the fuel cell impedance. Yet as mentioned above, the location of the MPP in the I–P plane is hard to predict. How to control the variable load to track the MPP is thus a rather challenging task.

Up to now, few researches on fuel cell MPPT control have been reported, but a number of methods have been used in photovoltaic power applications [7], such as the perturbation and observe (P&O) method, the conductance incremental method, the parasitic capacitance method, the only current method, model-based methods, and artificial intelligence methods. Among them the P&O algorithm is by far the most commonly used in practice because of its ease of implementation [8]. But due to the limitation that P&O exhibits erratic instable behavior under rapidly changing environments, the algorithm is unsuitable for the job of tracking the frequently moving MPP [9].

In this paper, a maximum power point tracking (MPPT) controller is designed, which can be used to adjust the load to the source impedance so that the equilibrium operating point coincides with the fuel cell's MPP. In order to operate the fuel cell at its MPP for every instant, the MPPT controller is made up of an adaptive feedback extremum seeking algorithm and a switch mode power regulator. The purpose of the extremum seeking method is to iteratively adjust the fuel cell's current and thus steer the operating point to the maximum of the I–P plane which corresponds to a maximum output power. The power regulator forces the fuel cell to work with the reference current given by the extremum seeking algorithm.

Extremum seeking is an adaptive non-linear control method which has been used since 1950s, but theoretical foundations for its stability and performance were established just recently by Krstic and Wang [10]. The approach enjoys two main advantages when applied to fuel cell MPPT control. Firstly, it does not require any prior knowledge of the fuel cell; secondly, according to the adaptive control law, the MPP will definitely be achieved when the control is convergent.

The paper is organized as follows. A dynamic model of PEM fuel cells is presented in Section 2; and in Section 3 an adaptive MPPT controller is designed. In Section 4 extremum seeking is applied to the fuel cell power system and simulation results are discussed in detail.

2. Fuel cell power performance curve analysis

2.1. Fuel cell simulation model

2.1.1. Dynamic gas transport model

The proportional relationship between the flow of gas through a valve and the partial pressure can be stated as [11]

$$\frac{q_{H_2}}{P_{H_2}} = \frac{k_{an}}{\sqrt{M_{H_2}}} = k_{H_2} \tag{1}$$

and

$$\frac{q_{O_2}}{P_{O_2}} = \frac{k_{an}}{\sqrt{M_{O_2}}} = k_{O_2} \tag{2}$$

where q_{H_2} is molar flow of hydrogen (kmol S^{-1}), P_{H_2} hydrogen partial pressure (atm), k_{H_2} hydrogen valve molar constant (kmol(atm S)$^{-1}$), k_{an} anode valve constant ($\sqrt{k\,\mathrm{mol\,kg}}$ (atm s)$^{-1}$), M_{H_2} molar mass of hydrogen (kg kmol^{-1}).

For hydrogen, the derivative of the partial pressure can be calculated by using the following perfect gas equation

$$\frac{\mathrm{d}}{\mathrm{d}t}P_{H_2} = \frac{RT}{V_{an}}(q_{H_2}^{in} - q_{H_2}^{out} - q_{H_2}^{r}) \tag{3}$$

where R is the universal gas constant ((1 atm) (kmol K)$^{-1}$)), T absolute temperature (K), V_{an} anode volume (1), $q_{H_2}^{in}$ hydrogen input flow (kmol S^{-1}), $q_{H_2}^{out}$ hydrogen output flow (kmol S^{-1}), $q_{H_2}^{r}$ hydrogen flow that reacts (kmol S^{-1}).

The amount of hydrogen consumed in the reaction can be calculated from the following electrochemical principle:

$$q_{H_2}^{r} = \frac{NI}{2F} = 2k_r I \tag{4}$$

where N is the number of the series-wound fuel cells in the stack, I the stack current (A), F Faraday's constant (C kmol^{-1}), k_r modeling constant (kmol(sA)$^{-1}$).

When the output flow is replaced by Eq. (1) and the Laplace transform is applied to Eqs. (3) and (4), hydrogen partial pressure can be rewritten in the s domain as:

$$P_{H_2} = \frac{1/k_{H_2}}{1+\tau_{H_2}s}(q_{H_2}^{in} - 2k_r I) \tag{5}$$

where

$$\tau_{H_2} = \frac{V_{an}}{k_{H_2}RT} \tag{6}$$

By the same means, the equations for oxygen partial pressure can be derived as:

$$P_{O_2} = \frac{1/k_{O_2}}{1+\tau_{O_2}s}(q_{O_2}^{in} - k_r I) \tag{7}$$

where

$$\tau_{O_2} = \frac{V_{ca}}{k_{O_2}RT} \tag{8}$$

Eq. (5) describes the relationship between stack current and hydrogen partial pressure, and Eq. (7) the relationship between stack current and oxygen partial pressure. As the load draws current, the reactants – hydrogen and oxygen – become depleted in the fuel cell stack, and both partial pressures drop accordingly. To protect the fuel cell plant from reactants starvation, commonly excessive amounts of hydrogen and oxygen are provided for the stack ($q_{H_2}^{in} > 2k_r I$, $q_{O_2}^{in} > k_r I$). A higher excess ratio leads to higher partial pressures, and then a higher fuel cell voltage. However, too much excess flow is a problem as it dries out the membrane and consumes much more parasitic power. Pukrushpan et al. [12] did a high quality study on how to control the excess ratio. They designed several air flow controllers to regulate the input flow rate so that it is always twice as much as the reaction rate. To focus on the MPPT control problem, this paper will not go into details on the excess ration control issue but simply supply the fuel cell with a constant flow rate that is sufficient for consumption.

2.1.2. Polarization curve model

The fuel cell voltage as a function of current density in a steady state can be represented by a polarization curve, which is influenced by such parameters as the cell temperature, oxygen partial pressure, hydrogen partial pressure and membrane water content. When current is drawn from a fuel cell, the cell voltage V_{cell} decreases from its equilibrium thermodynamic potential E_{nernst} (open circuit voltage). This voltage drop consists of activation loss η_{act}, ohmic loss η_{ohmic} and concentration loss η_{con}. The basic expression for the cell voltage is:

$$V_{cell} = E_{nernst} + \eta_{act} + \eta_{ohmic} + \eta_{con} \tag{9}$$

Reversible thermodynamic potential E_{nernst} is described by the Nernst equation. With literature values for the standard-state entropy change, the expression is [13]:

$$E_{nernst} = 1.229 - 8.5\times10^{-4}(T-298.15) + 4.308 \times 10^{-5}T(\ln P_{H_2} + 0.5\cdot\ln P_{O_2}) \tag{10}$$

Activation overvoltage η_{act} is described by the Tafel equation, which can be expressed as [13]

$$\eta_{act} = \xi_1 + \xi_2 T + \xi_3 T \ln C_{O_2} + \xi_4 T \ln I \tag{11}$$

where $\xi(i=1\text{–}4)$ are parametric coefficients for each cell model. C_{O_2} is the concentration of dissolved oxygen at the gas/liquid interface (mol cm^{-3}), which can be calculated by means of

$$C_{O_2} = \frac{P_{O_2}}{(5.08\times10^6)\times\exp(-498/T)} \tag{12}$$

Ohmic overvoltage η_{ohmic} results from the resistance of the polymer membrane in electron and proton transfers. It can be expressed as

$$\eta_{ohmic} = -IR_m \tag{13}$$

The ohmic resistance R_m is given by

$$R_m = \frac{r_m t_m}{A} \tag{14}$$

where r_m is membrane resistivity (Ω cm) to proton conductivity, t_m membrane thickness (cm), A cell active area (cm^2). Membrane resistivity depends strongly on membrane humidity and temperature, and can be described by the following empirical expression [14]

$$r_m = \frac{181.6\left[1+0.03(I/A)+0.0062(T/303)^2(I/A)^{2.5}\right]}{\left[\lambda_m - 0.634 - 3(I/A)\right]\exp\left[4.18(T-303/T)\right]} \tag{15}$$

where λ_m is the membrane water content. The membrane water content is a function of the average water activity a_m:

$$\lambda_m = \begin{cases} 0.043 + 17.81a_m - 39.85a_m^2 + 36a_m^3, & 0 < a_m \le 1 \\ 14 + 1.4(a_m - 1), & 1 < a_m \le 3 \end{cases} \tag{16}$$

The average water activity is related to the anode water vapor partial pressure $P_{v,an}$ and the cathode water vapor partial pressure $P_{v,ca}$:

$$a_m = \frac{1}{2}(a_{an+}a_{ca}) = \frac{1}{2}\frac{P_{v,an}+P_{v,ca}}{P_{sat}} \tag{17}$$

The saturation pressure of water P_{sat} can be figured out with the following empirical expression:

$$\log_{10}P_{sat} = -2.1794 + 0.02953T - 9.1813\times10^{-5}T^2 + 1.4454\times10^{-7}T^3 \tag{18}$$

The value of λ_m varies between 0 and 14, which is equivalent to the relative humidity of 0% and 100%. Under supersaturated conditions, however, the maximum possible value of λ_m can be as high as 23. In addition, λ_m can also be influenced by the membrane preparation procedure, the relative humidity of

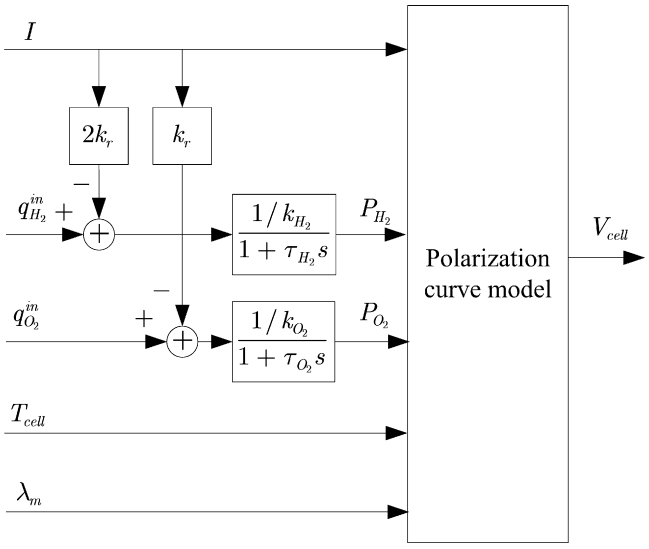

Fig. 2. PEM fuel cell simulation model.

the feed gas, the stoichiometric ratio of the feed gas, and the age of the membrane [15]. Hence, in this paper, λ_m is considered as an adjustable parameter with a possible value between 0 and 23.

Concentration overvoltage η_{con} results from the concentration gradient of reactants as they are consumed in the reaction. The equation for concentration overvoltage is shown by [16]

$$\eta_{con} = \frac{RT}{nF} \ln\left(1 - \frac{I}{i_L A}\right) \tag{19}$$

where i_L is the limiting current. It denotes the maximum rate at which a reactant can be supplied to an electrode.

Combining the dynamic gas transport model and the static polar curve model together gives birth to a whole fuel cell simulation model, as shown in Fig. 2. The model parameters are listed in Table 1.

Table 1
Model parameters

Parameter	Value	Ref.
F (C kmol^{-1})	96484600	
R (J kmol^{-1} K)	8314.47	
N	35	[14]
A (cm^2)	232	[14]
$k_r = N/4F$	9.07×10^{-8}	
K_{H_2} (kmol s^{-1} atm)	4.22×10^{-5}	[11]
K_{O_2} (kmol s^{-1}atm)	2.11×10^{-5}	[11]
τ_{H_2}(s)	3.37	[11]
τ_{O_2}(s)	6.47	[11]
t_{mem} (cm)	0.0178	[14]
ξ_1	−0.944	[14]
ξ_2	0.00354	[14]
ξ_3	7.8×10^{-8}	[14]
ξ_4	-1.96×10^{-4}	[14]
i_L (A cm^{-2})	2.0	Assumed

2.2. Power performance curve analysis

The output power of the fuel cell stack can be calculated by the expression

$$P_{stack} = NV_{cell}I \tag{20}$$

and the power characteristic of the external load R_L is

$$P_{load} = I^2 R_L \tag{21}$$

As an example, Fig. 3 shows the fuel cell stack power performance curves when the membrane water content is 12 and 16 and the load is 0.065 Ω and 0.03 Ω. The other working conditions are the temperature of 70 °C, the oxygen pressure of 1 atm, and the hydrogen pressure of 1 atm. It can be seen clearly that:

- The operating point is at the intersection of the fuel cell power curve and the load power curve. Thus the power delivered takes a unique value based on both the load resistance and the fuel cell operation parameters.
- There exists a unique maximum power point, at which the fuel cell produces maximum power.

When the membrane water content is 12, fuel cell produces a maximal power of 3812 W with a load resistance of 0.065 ohm. If the load resistance is changed to 0.03 ohm, the working point moves from A to B, and the power drops from 3812 to 3181 W. This means only 83% of the power potential is used. If the membrane water content increases from 12 to 16, the working point shifts from A to C, and thus the power rises from 3812 to 4735 W, 97% of the possible maximal 4864 W.

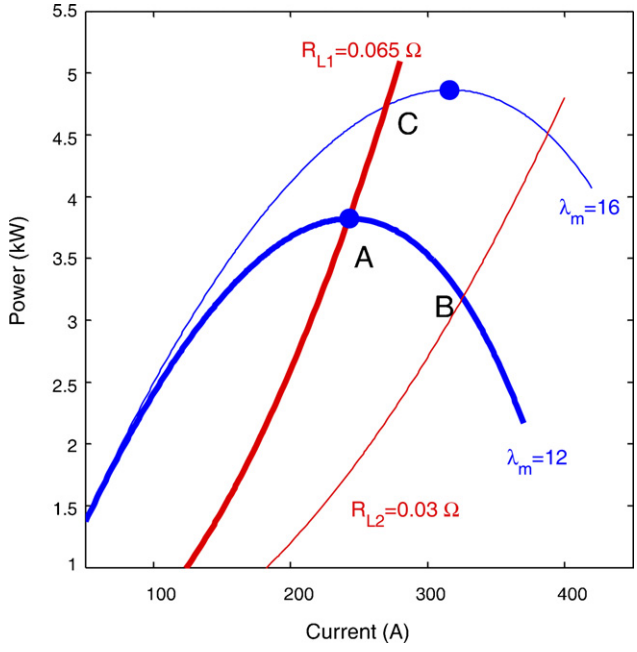

Fig. 3. The PEM fuel cell power curves under different operation conditions. Oxygen pressure and hydrogen pressure are both regulated to 1 atm.

3. Adaptive MPPT controller design

3.1. Schematic of the fuel cell MPPT control system

Since the power available from the fuel cell is limited, it is necessary to adjust the operation point to settle on or trace the maximum power points. The majority of fuel cell control literature is focused on regulating and tracking system states to known setpoints or trajectories. Thus the specific MPPs can be chosen a priori by solving a steady-state optimization problem subject to operational constraints. In this way, the optimality of such operating policies is completely dependent on the quality of the fuel cell model. Besides the model mismatch, the fuel cell operation strongly depends in a nonlinear way on many operating parameters, some of which are even unmeasurable. Owing to the uncertainty and time-varying dynamic properties of the electrochemical processes, the MPPs chosen a priori will be suboptimal, and can be improved by performing the optimization in real time. When fuel cell models are not well defined or when only limited operation parameter measurements are available, it is necessary to consider a model-free MPPT control, which is able to automatically tune the working point in the right direction. Fig. 4 shows the schematic of the proposed two-level MPPT control system.

Changing the fuel cell operating parameters can shift the working point, but regulating the external load impedance is more effective to locate the MPP. Thus the fuel cell operating parameters are usually used to maintain good working conditions. An additional power conditioner between the fuel cell and the load can change the equivalent load impedance. A supervisory MPPT controller functions primarily as an MPP searching unit, deciding the fuel cell working point. The lower-level DC-DC controller receives commands from the supervisory MPPT controller and then generates detailed control instructions for the power conditioning circuit.

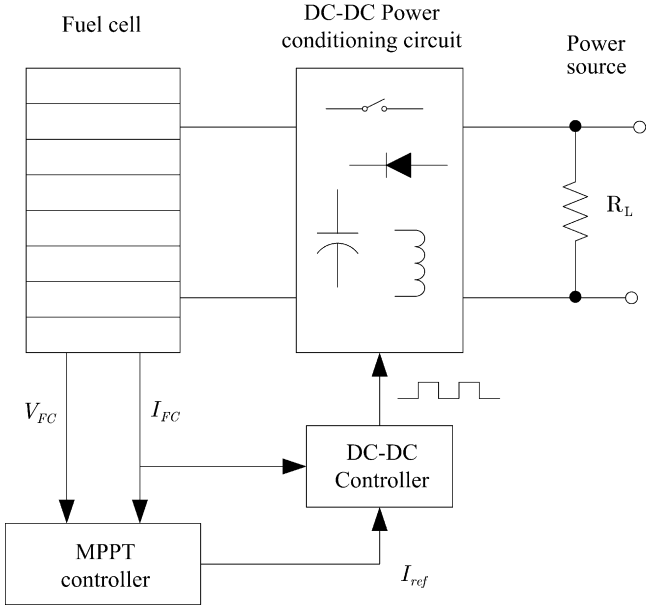

Fig. 4. Schematic of the fuel cell MPPT control system.

The current mode power conditioner can efficiently transform a regulated DC output power from a fluctuating fuel cell source power to a variable load resistance in an appropriate form. The converter with a variable current gain G will result in the fuel cell seeing an equivalent load resistance.

$$R_{\text{equ}} = G^2 R_{\text{L}} \tag{22}$$

Therefore a feedback MPP tracking algorithm iteratively regulates the fuel cell current with the power conditioner, and the power conditioner forces the fuel cell to work at the current by shifting the equivalent load impedance. When the current coincides with the MPP, the equivalent load impedance matches the internal resistance of the fuel cell.

The current in the DC-DC converter is generally controlled by a switching concept. The power switch MOSFET Q can be turned on or off in a controlled fashion, and the average current is a function of the on-time of the switch, the pulse width, and the switching frequency. The most common techniques of controlling a converter are pulse-width modulation [17] and sliding-mode control [18]. The power converter transient can settle in milliseconds [19], which is sufficiently brief to be safely ignored. Thus, the converter can be treated as a direct through unit which is able to instantaneously regulate the fuel cell current to commands from the MPP tracing algorithm.

3.2. Perturbation and observe (P&O) control algorithm

The fuel cell working point is mainly determined by the supervisory MPPT control algorithm. Although few discussions on MPPT control for fuel cells can be found, a number of MPPT methods have been proposed in photovoltaic power applications. Among them, the perturbation and observe (P&O) algorithm, also known as the "hill climbing" method, is by far the most commonly used in practice because of its simplicity in algorithm and ease of implementation. The current based P&O algorithm tracks the peak-power current on the basis of the past fuel cell currents and powers. Fig. 5 shows the basic form of the P&O algorithm. The operating current of the fuel cell is perturbed by a small constant increment, and the resulting change of power, ΔP, is observed. If ΔP is positive, then it is supposed that it has moved the operating point closer to the MPP. In this case, further current perturbations in the same direction will move the operating point toward the MPP. If ΔP is negative, then the operating point has moved away from the MPP, and the direction of perturbation should be reversed to move back toward the MPP.

Many improvements on the P&O algorithm have been proposed. For example, a variable step size of perturbation with the slope of power as a variable is as follows [20]:

$$I[k+1] = I[k] + M\frac{\Delta P[k]}{\Delta I[k]} \tag{23}$$

where M is the step-size corrector, and $\Delta P[k]/\Delta I[k]$ denotes the instantaneous power gradient at the Kth sampling period. In order to find the direction of change for maximizing the power, the P&O method periodically perturbs the operation point of

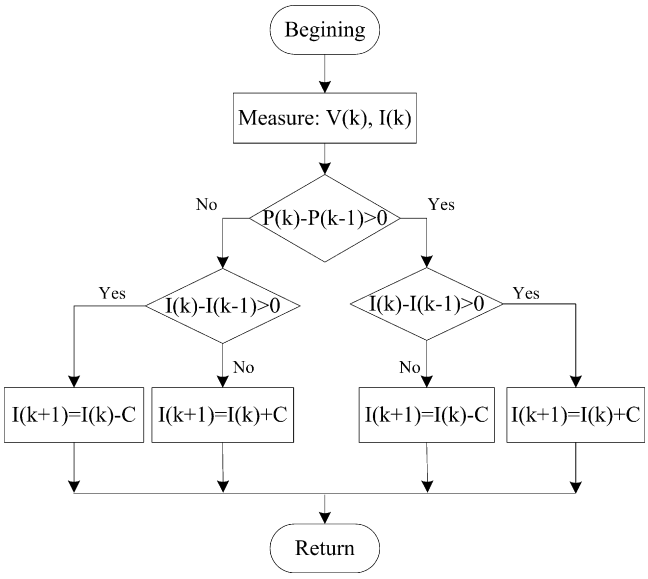

Fig. 5. Flowchart of the P&O algorithm. C is the step of the perturbation.

the system. If the sign of power derivative ΔP and that of voltage derivative ΔI are the same, the reference current should be further increased, and vice versa.

A major problem of the traditional numerically based MPP control methods is that they are lacking in solid theoretical support. As a result, their stability and robustness is hard to analyze and may deteriorate in some unfavorable environments. The P&O method, for example, requires the plant dynamics settle down before optimization. It works well under static conditions but exhibits erratic behaviors under rapidly changing conditions. For instance, an abrupt change in membrane water content will be followed by an immediate change of power. This leads to $\Delta P[k]/\Delta I[k] \to \infty$ and makes the step size too big, as shown in Eq. (23).

3.3. Theory of the proposed adaptive MPPT controller for fuel cell systems

Recently, Krstic et al. [10,21] presented a systematic extremum-seeking control methodology supported by such rigorous theories as averaging and singular perturbation. This real-time optimization methodology involves a nonlinear dynamic system with feedback and adaptation. These features render the extremum-seeking-based algorithm more effective than classical optimization and adaptive control algorithms in many advanced applications, such as traction maximization in antilock braking for a car [22], productivity maximization of a continuous stirred tank bioreactor [23], power reduction maximization of a flight [24], pressure rise maximization of an aeroengine compressor [25], autonomous vehicle target tracking [26], and PID tuning [27].

As compared with classical numerically based MPPT methods, the extremum-seeking control approach enjoys two advantages. Firstly, the optimization problem of power maximization is explicitly solved by using the dynamic adaptation-based feedback control law with sinusoidal perturbation. The MPP is hence guaranteed to be achieved when the control is convergent. Secondly, extremum seeking is a nonmodel-based adaptive control method that can be used to find an unknown, optimal operating condition for the nonlinear system, where the nonlinearity has a local minimum or maximum. In other words, our approach does not require any parameterization or structural formalization of the modeling uncertainty.

With the self-optimizing extremum algorithm as the MPPT controller, the control objective is for the fuel cell operating point to rapidly trace the MPPs subject to uncertainties and disturbances from the fuel cell and the external load. A block diagram for extremum seeking implemented on a fuel cell system is shown in Fig. 6. I_{ref} is our estimation of the unknown MPP current I_{max}, at which the fuel cell produces maximum power P_{max}. a, ω and ϕ are the amplitude, frequency and phase shift of the probing signal, respectively. ω_h is the cut-off frequency of the high-pass filter. k is the positive adaptive gain of the integrator. $C(s)$ is the compensator.

For the sake of clarity, this paper only deals with a controller with $C(s) = 1$ and $\phi = 0$, as given in Fig. 7. This controller design is the simplest form of an extremum-seeking algorithm where the algorithm does not employ any compensation or demodulator phase shift. Although the MPPT controller appears to be extremely simple, the analysis of the scheme is indeed intricate. The MPPT controller locates the MPP by injecting a small-signal periodical sinusoidal perturbation into the current I_{ref}. If the perturbation frequency is sufficiently large, the fuel cell will appear like a static map and its dynamics do not interfere with the MPPT controller. The small perturbation will create a response of P. Then the high-pass filter and the integrator are applied to eliminate the static component of power and extract the gradient information.

An elementary intuitive verification is given as follows. It consists of two steps: first, it is proved that the MPPT controller can drive the fuel cell from any working point to the MPP; second, that the MPP is an equilibrium point is proved.

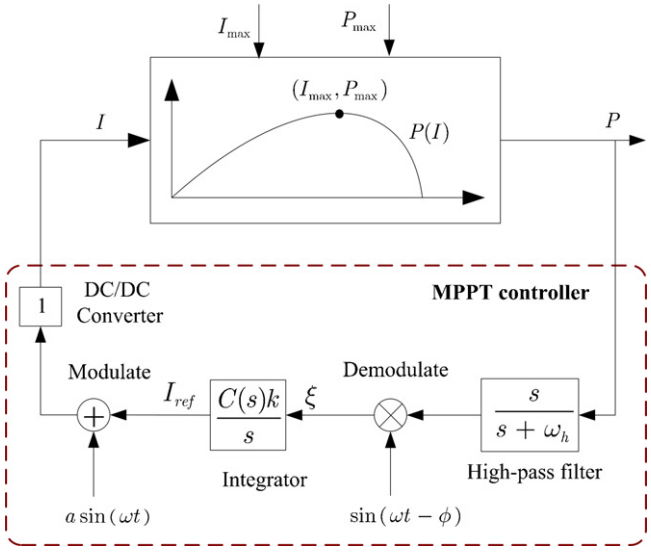

Fig. 6. MPPT controller scheme for the fuel cell system.

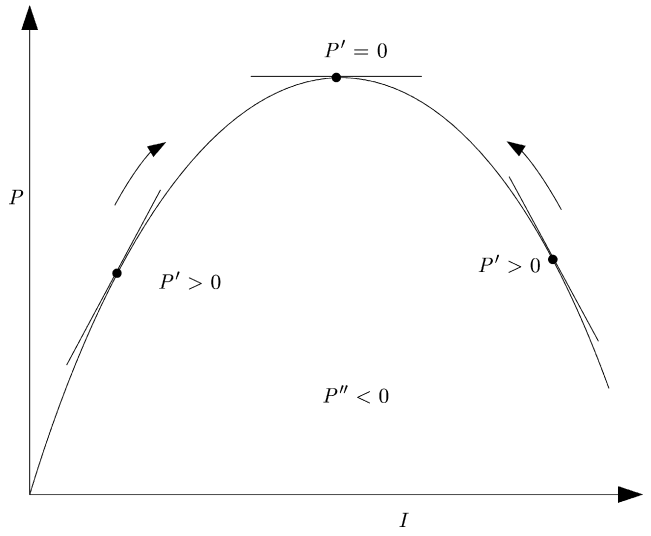

Fig. 7. Variation of the dP/dI on the P–I curve.

The following calculations drive home the point that starting from any point (P_0, I_0) at time t_0, the MPPT controller can use the small modulated perturbation to determine the slope of the power versus current curve and drive the system to the MPP. The power response to the perturbation signal at P_0 can be approximated by the Taylor series

$$P = P_0 + P'(I_0 + a\sin\,\omega t) + \frac{P''}{2!}(I_0 + a\sin\,\omega t)^2 + \cdots \quad (24)$$

After dropping the second and higher order terms, Eq. (24) can be rewritten as

$$P = P_0 + P'I_0 + aP'\sin\,\omega t \quad (25)$$

The MPPT controller applies the high-pass filter $s/(s+h)$ to the output power P to eliminate the slowly changing DC component $P_0 + P'I_0$:

$$\frac{1}{s+h}[P] = aP'\sin\,\omega t \quad (26)$$

This signal is then demodulated by multiplication with $\sin\,\omega t$:

$$\xi = aP'\sin^2\,\omega t = \frac{aP'}{2} - \frac{aP'}{2}\cos\,2\omega t \quad (27)$$

With the initial value of the integrator being I_0, the estimated current is

$$\begin{aligned} I_{\text{ref}} &= k\int \xi \mathrm{d}t \\ &= I_0 + \frac{ka}{2}P't - \frac{kaP'}{2}\int \cos\,2\omega t\mathrm{d}t \end{aligned} \quad (28)$$

Noting that the second term in Eq. (28) is a high frequency periodical signal around zero, which can be attenuated by the integrator, we get

$$I_{\text{ref}} = I_0 + \frac{ka}{2}P't \quad (29)$$

As shown in Fig. 7, if the value of I_0 is smaller than that of $I_{\max}$, the working point is at the left side of the MPP, and thus $P' > 0$. The current increment $kaP't/2$ is accordingly a positive value, and the working point will move to MPP. Contrarily, if I_0 is bigger than $I_{\max}$, the current will decrease to $I_{\max}$ because of $kaP't/2 < 2$.

To prove that once the working point arrives at the MPP, the MPPT controller can stabilize the system in the small neighborhood of the MPP, we start with defining the estimation error of current as:

$$I_e = I_{\max} - I_{\text{ref}} \quad (30)$$

A well designed MPPT controller should force e to converge to zero. The fuel cell $P(I)$ function can be approximated in the neighborhood of the MPP by Taylor series

$$P = P_{\max} + P'(I - I_{\max}) + \frac{P''}{2!}(I - I_{\max})^2 + \cdots \quad (31)$$

We also can get

$$I - I_{\max} = I - I_{\text{ref}} - I_e = a\sin\,\omega t - I_e \quad (32)$$

With Eq. (32), Eq (31) can be written as

$$P = P_{\max} + P'(a\sin\,\omega t - I_e) + \frac{P''}{2!}(a\sin\,\omega t - I_e)^2 + \cdots \quad (33)$$

Obviously $P' = 0$ at the MPP, and by dropping the higher order terms, Eq. (31) can be rewritten as

$$P = P_{\max} + \frac{1}{2}P''(I - I_{\max})^2 \quad (34)$$

With Eq. (32), Eq. (34) can be written as

$$\begin{aligned} P &= P_{\max} + \frac{P''}{2}(a\sin\,\omega t - I_e)^2 \\ &= P_{\max} + \frac{a^2P''}{4} + \frac{P''}{2}{I_e}^2 \\ &\quad - aP''I_e\sin\,\omega t - \frac{a^2P''}{4}\cos\,2\omega t \end{aligned} \quad (35)$$

Estimation error I_e is a very small value in the neighborhood of the MPP, thus its quadratic term I_e^2 in Eq. (35) can be neglected. The MPPT controller applies the high-pass filter $s/(s+h)$ to the output power P to eliminate the slowly changing DC component $P_{\max} + a^2P''/4$:

$$\frac{1}{s+h}[P] = -aP''e\sin\,\omega t - \frac{a^2P''}{4}\cos\,2\omega t \quad (36)$$

This signal is then demodulated by multiplication with $\sin\,\omega t$

$$\begin{aligned} \xi &= -aP''I_e\sin^2\,\omega t - \frac{a^2P''}{4}\sin\,\omega t\cos\,2\omega t \\ &= -\frac{a^2P''}{2}I_e + \frac{a^2P''}{2}I_e\cos\,2\omega t \\ &\quad - \frac{a^2P''}{8}(\sin\,\omega t - \sin\,3\omega t) \end{aligned} \quad (37)$$

The estimated current is

$$I_{\text{ref}} = k\int \xi \mathrm{d}t = -\frac{ka^2P''}{2}\int e\mathrm{d}t + \int\left[\frac{a^2P''}{2}e\cos 2\omega t - \frac{a^2P''}{8}(\sin\omega t - \sin 3\omega t)\right]\mathrm{d}t \quad (38)$$

The second term in Eq. (38) can be attenuated by the integrator, thus

$$I_{\text{ref}} = -\frac{ka^2P''}{2}\int I_e\mathrm{d}t \quad (39)$$

Eq. (39) can be rewritten as

$$\dot{I}_{\text{ref}} = -\frac{ka^2P''}{2}I_e \quad (40)$$

Because $I_{\max}$ is a constant, we can get $\dot{I}_{\text{ref}} = -\dot{I}_e$ from Eq. (30). Thus

$$\dot{I}_e = \frac{ka^2}{2}P''I_e \quad (41)$$

Since $P(I)$ is a convex function with maximum, its second order derivative P'' should be negative, and $ka^2P''/2 < 0$. Thus we conclude that $I_e \to 0$, which means that the fuel cell current converges to $I_{\max}$ and the MPPT controller drives the output power to the neighborhood of $P_{\max}$.

According to the theory put forward by Krstic et al. [10], there exists a ball of initial conditions around the point $(I,P,\xi) = (I_{\max}, P_{\max}, 0)$ and constants $\bar{\omega}$, $\bar{\delta}$ and $\bar{a}$ such that for all $\omega \in (0, \bar{\omega})$, $\delta \in (0, \bar{\delta})$ and $a \in (0, \bar{a})$, the solution $(I(t), P(t), \xi(t))$ exponentially converges to an $O(\omega + \delta + a)$-neighborhood of that point.

3.4. Design consideration of the adaptive fuel cell MPPT controller

The choice of the control system parameters affects the system performance. As we can see from the above analysis, the overall fuel cell MPPT control system should have three time scales:

- fastest—the periodic perturbation,
- medium—the high-pass filter,
- slow—the fuel cell.

Thus the periodical sinusoidal perturbation signal frequency ω and the high-pass filter cut-off frequency ω_{h} are chosen as follows:

$$\omega \gg \omega_{\text{h}} \gg \text{dynamic speed of fuel cell with controller} \quad (42)$$

A higher ω can separate the perturbation signal from the fuel cell dynamic response clearly. But if ω is selected too high, the convergence speed will become too slow. Thus, ω should be selected to the degree that it is just sufficient to satisfy Eq. (42).

The value of Ka^2 has a significant effect on the system convergence speed as shown in Eq. (41). A small Ka^2 slows down the convergence. Increasing the adaptation gain k or the perturbation signal amplitude a can improve the tracking speed, but the system will become more sensitive to noise or ripple contents. Therefore a moderate ka^2 should be used.

4. Simulation results and discussion

The complete fuel cell MPPT control system block diagram is shown in Fig. 8. The fuel cell is modeled as shown in Fig. 2, while the whole MPPT control system is written and tuned by simulations on the Simulink/Matlab environment. The current and power of fuel cell stacks varies with their active area and number of cells, and this variation will influence the selection of controller parameters. To enlarge the scope of our research application, noting that the current densities and the power densities of different fuel cells are similar, we design the MPPT controller on the basis of current density and power density instead of current and power.

It is crucial to note that all of the static or dynamic fuel cell characteristics can be unknown. The fuel cell model presented

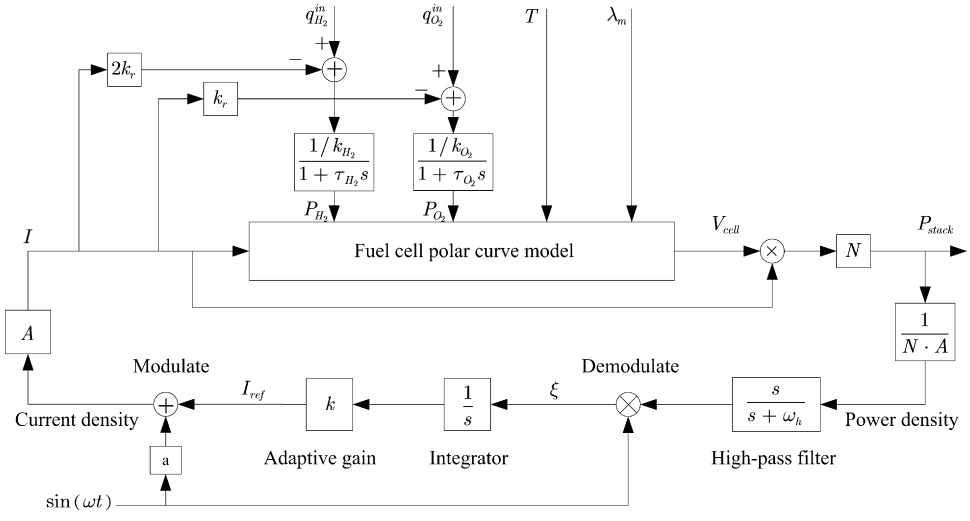

Fig. 8. Fuel cell MPPT control system block diagram.

in Section 2.1 must be viewed as a theoretical benchmark to illustrate and analyze the efficiency of the proposed MPPT control approach. Even the black-box neuron network model [28] or the support vector machine model [29] can also be used here. It is also to note that a stably operated fuel cell plant needs a group of controllers. In addition to the excess ratio controller mentioned earlier, water and heat subsystems also need to be properly controlled. In the following simulations, it is assumed that they have already been well controlled.

The basic simulation conditions of the fuel cell are: hydrogen input flow of 8×10^{-5} kmol s^{-1}, oxygen input flow of 4×10^{-5}kmol s^{-1}, cell temperature of 70 °C and membrane water content of 14. The parameters of the MPPT control system are: $a = 5$, $\omega = 2\pi$, $k = 14$ and $\omega_h = \pi$.

Fig. 9 shows the fuel cell MPPT control system's responses to step changes of the membrane water content. It is important to understand that these abrupt changes of the membrane water content are for testing the dynamic response of the MPPT control system, and do not necessarily represent changes in a real world case. The membrane water content abruptly changes from 8 to 12 at the 100th second, from 12 to 16 at the 150th second and from 16 back to 12 at the 200th second, as shown in Fig. 9a. The corresponding MPPs also move from point A to B, from B to C and then from C back to B, as shown in Fig. 10a.

Figs. 9 and 10 show that the MPPT controller can steadily drive the system to the new MPP when an abrupt change of the MPP occurs. For example, when the membrane water content abruptly changes from 8 to 12 at the 100th second, the fuel cell operating point immediately shifts to point A′, and the MPP shifts to point B′. If the P&O algorithm governed by Eq. (23) is used, the step change of power from point A to A′ will lead to $\Delta P[k]/\Delta I[k] \to \infty$, and then the P&O algorithm will collapse. The MPPT controller, however, can converge to the maximum power point B smoothly, as shown in Fig. 9f and 10b.

The movement from point B′ to B is caused by the couple between current and oxygen/hydrogen pressures, as described by Eqs. (5) and (7). When the current rises, the depletion of the reactant gases increases, and the gas pressures decrease, as shown in Fig. 9d and e. And when the reactant pressures change, the location of the MPP changes accordingly, as described in Section 2.1.2. Strictly speaking, the membrane water content and the fuel cell temperature both vary with current. When current is changed to seek the MPP, the location of the MPP changes correspondingly. But the MPPT control system is robust enough to trace the locus of MPPs until the equilibrium point B is reached.

Fig. 11 shows the fuel cell MPPT control system's ramp response to the temperature. The fuel cell temperature rises from 20 to 90 °C at the rate of 0.1 °C s^{-1}. When the temperature changes from 20 to 90 °C, the MPP moves from Point A to B. The MPPT control system traces the theoretical MPP locus at the same time. The tracing error is mainly caused by the slow change of the gas pressures.

Although this MPPT controller leads to a forced oscillation current, it achieves a very low power oscillation around the MPP. A periodical perturbation current of $a\sin\omega t$ is injected to the fuel cell current. This leads to a ripple power, whose amplitude depends on the relative location of the operation point to the

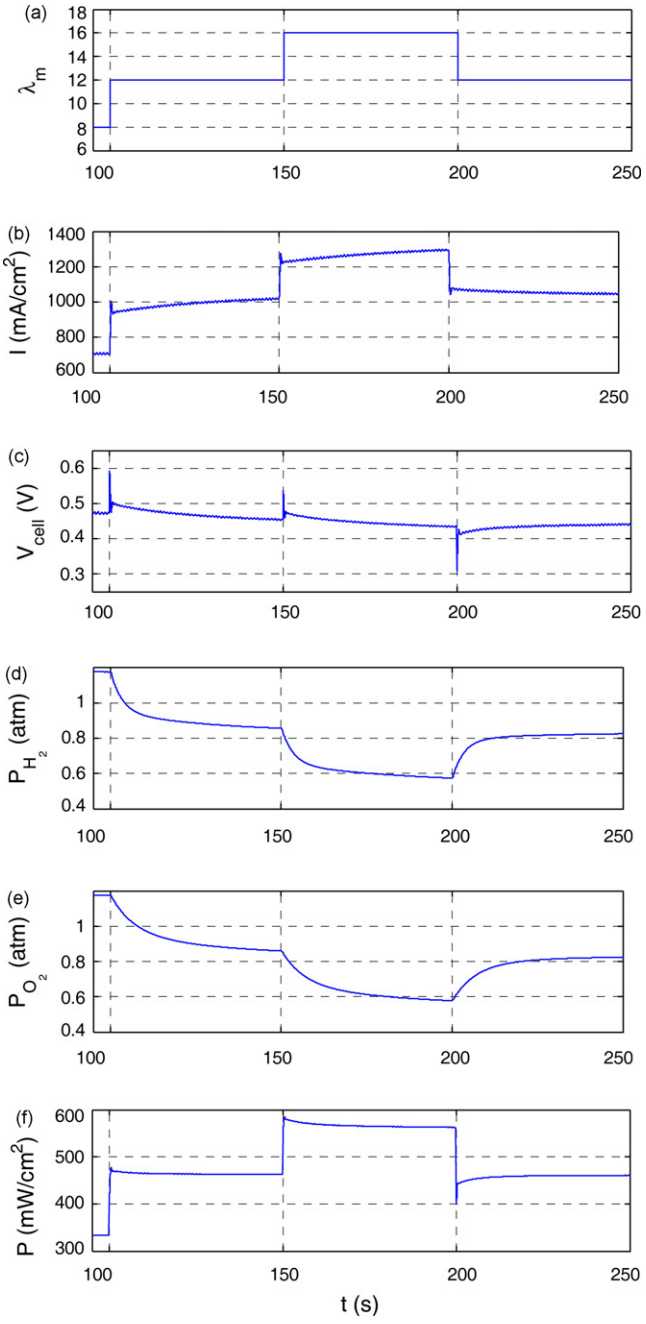

Fig. 9. Responses of the MPPT controller to the step changes of membrane water content: (a) step changes of membrane water content; (b) responses of current density; (c) responses of cell voltage; (d) responses of hydrogen pressure; (e) responses of oxygen pressure; (f) responses of power density.

MPP. The power oscillation amplitude can be approximated by

$$\text{Power amplitude} = \frac{\mathrm{d}P}{\mathrm{d}I} \times a \tag{43}$$

As mentioned earlier, $\mathrm{d}P/\mathrm{d}I \to 0$ at the MPP. Thus the power amplitude will converge to zero at the MPP. Fig. 10b shows that the power ripple becomes lower and lower when the operation point gets close to MPP B. Fig. 12 gives a clearer picture when the operation point is very close to MPP B. The current ripple factor in Fig. 12a is about 1%, but the corresponding power ripple factor is only 0.02% as shown in Fig. 12b.

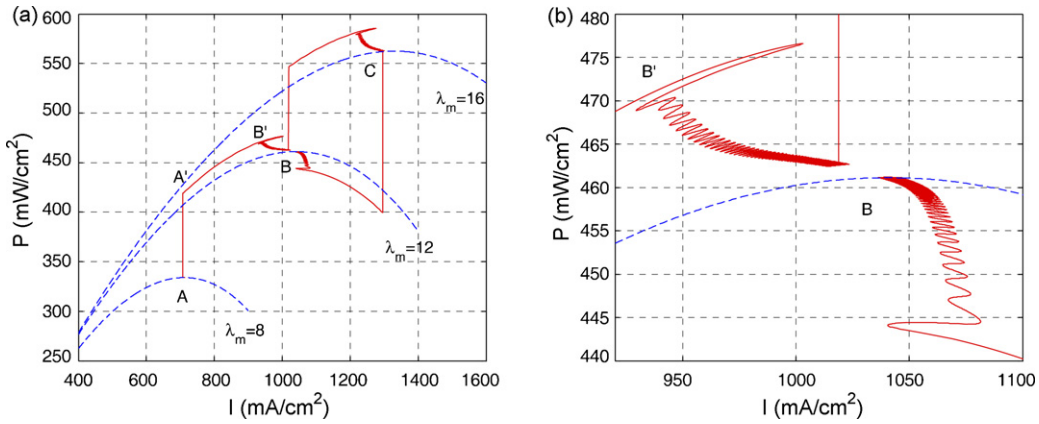

Fig. 10. Power responses in phase plan of power density versus current density: (a) power density responses in I–P plan; (b) oscillations nearby point B. Dot lines are the polar curves at different membrane water contents.

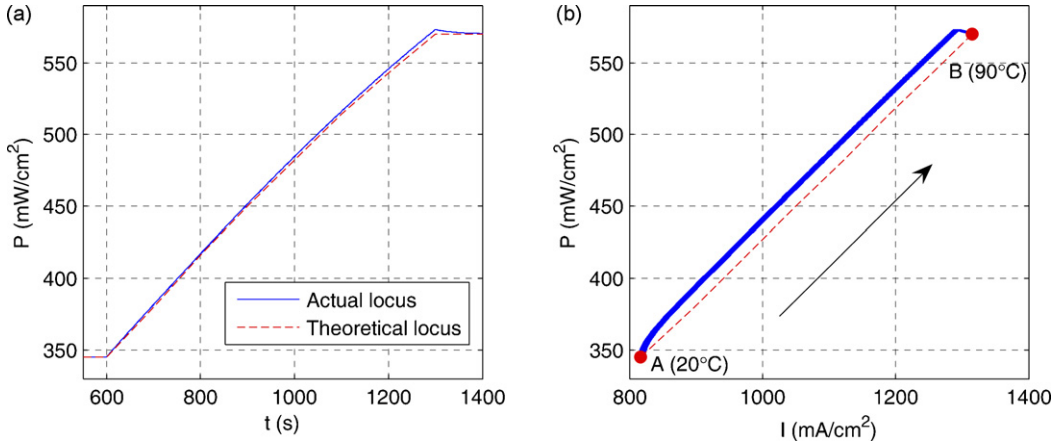

Fig. 11. Response of the MPPT controller to the ramp change of temperature: (a) power density responses in time domain; (b) power density responses in I–P plan.

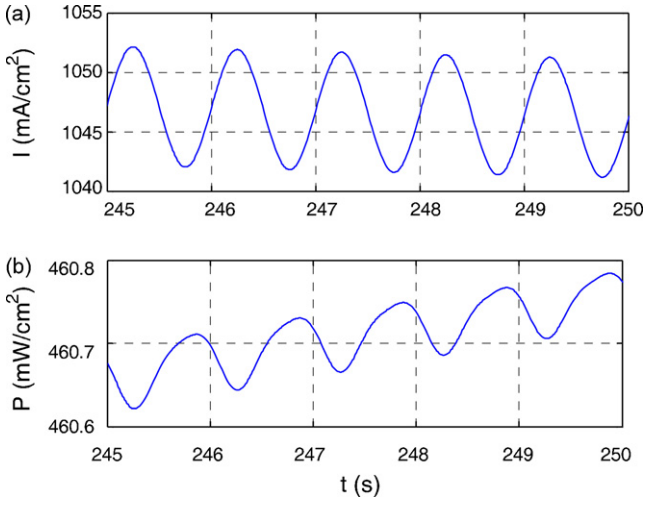

Fig. 12. Ripples of Fuel cell MPPT control system.

5. Conclusion

A modeling, control, and simulation study of the fuel cell MPPT control system is reported in this paper. Firstly, a theoretical analysis of the power curve characteristic of the fuel cell is made. The fuel cell has a unique MPP, at which it produces maximum power. The location of the MPP is decided by fuel cell operation conditions in a nonlinear way. Due to the complexity of the electrochemical process, however, it is hard to predict whether the fuel cell is working at the MPP by a modeling approach.

Therefore, an adaptive MPPT controller using the extremum-seeking algorithm is designed to automatically keep the fuel cell working at the MPP all the time. The controller is based on solid dynamic adaptive control theories. The MPP is guaranteed to be achieved when the control is convergent. Also, this MPPT controller is a model-free method which does not require any prior knowledge of the fuel cell. The validity of the proposed fuel cell MPPT control scheme over a large operating range was verified through simulations in the MATLAB/Simulink environment. Simulation results show that the system can respond rapidly to abrupt changes of operation conditions.

The proposed control scheme can not only trace the MPP but also online solve other fuel cell optimization problems, such as maximize efficiency or combination of various objectives. We expect that it can be used in a large scope.

References

[1] V. Mishra, F. Yang, R. Pitchumani, J. Power Sources 141 (1) (2005) 47–64.

[2] C.Y. Wang, Chem. Rev. 104 (10) (2004) 4727–4765.
[3] A. Rowe, X.G. Li, J. Power Sources 102 (1–2) (2001) 82–96.
[4] A.Z. Weber, J. Newman, Chem. Rev. 104 (10) (2004) 4679–4726.
[5] A. Mawardi, F. Yang, R. Pitchumani, J. Fuel Cell Sci. Technol. 2 (2) (2005) 121–135.
[6] J.B. Benziger, M.B. Satterfield, W.H.J. Hogarth, J.P. Nehlsen, I.G. Kevrekidis, J. Power Sources 155 (2) (2006) 272–285.
[7] V. Salas, E. Olias, A. Barrado, A. Lazaro, Sol. Energy Mater. 90 (11) (2006) 1555–1578.
[8] D.P. Hohm, M.E. Ropp, Prog. Photovoltaics 11 (1) (2003) 47–62.
[9] T. Kawamura, K. Harada, Y. Ishihara, T. Todaka, T. Oshiro, H. Nakamura, M. Imataki, Sol. Energy Mater. 47 (1–4) (1997) 155–165.
[10] M. Krstic, H.-H. Wang, Automatica 36 (4) (2000) 595–601.
[11] M.Y. El-Sharkh, A. Rahman, M.S. Alam, P.C. Byrne, A.A. Sakla, T. Thomas, J. Power Sources 138 (1–2) (2004) 199–204.
[12] J.T. Pukrushpan, A.G. Stefanopoulou, H. Peng, IEEE Control Syst. Mag. 24 (2) (2004) 30–46.
[13] J.C. Amphlett, R.M. Baumert, R.F. Mann, B.A. Peppley, P.R. Roberge, T.J. Harris, J. Electrochem. Soc. 142 (1) (1995) 1–8.
[14] R.F. Mann, J.C. Amphlett, M.A.I. Hooper, H.M. Jensen, B.A. Peppley, P.R. Roberge, J. Power Sources 86 (1–2) (2000) 173–180.
[15] T.E. Springer, T.A. Zawodzinski, S. Gottesfeld, J. Electrochem. Soc. 138 (8) (1991) 2334–2342.
[16] Fuel Cell Handbook, 7th ed., EG&G Technical Services, Inc. U.S. Department of Energy, 2004.
[17] M. Giesselmann, H. Salehfar, H.A. Toliyat, T.U. Rahman, The Power Electronics Handbook, Industrial Electronics:, CRC Press, 2001 (Chapter 7).
[18] G. Spiazzi, P. Mattavelli, The Power Electronics Handbook, Industrial electronics, CRC press, 2001 (Chapter 8).
[19] F. Zenith, S. Skogestad, J. Process Control 17 (4) (2007) 333–347.
[20] P. Huynh, B.H. Cho, IEEE Trans. Aerosp. Electron. Syst. 32 (1) (1996) 182–190.
[21] M. Krstic, Syst. Control Lett. 39 (5) (2000) 313–326.
[22] H. Yu, U. Ozguner, Extremum-seeking control strategy for ABS system with time delay, in American Control Conference, 2002. Proceedings of the 2002, 5 (2002) 3753–3758.
[23] H.-H. Wang, M. Krstic, G. Bastin, Int. J. Adaptive Control Signal Process. 13 (8) (1999) 651–669.
[24] P. Binetti, K.B. Ariyur, M. Krstic, F. Bernelli, J. Guidance Control Dyn. 26 (1) (2003) 132–142.
[25] H.-H. Wang, S. Yeung, M. Krstic, IEEE Trans. Control Syst. Technol. 8 (2) (2000) 300–309.
[26] C. Zhang, A. Siranosian, M. Krstic, Automatica 43 (10) (2007) 1832–1839.
[27] N.J. Killingsworth, M. Krstic, IEEE Control Syst. Mag. 26 (1) (2006) 70–79.
[28] S. Jemei, D. Hissel, M.C. Pera, J.M. Kauffmann, J. Power Sources 124 (2) (2003) 479–486.
[29] Z.-D. Zhong, X.-J. Zhu, G.-Y. Cao, J. Power Sources 160 (1) (2006) 293–298.